Shape Reconstruction of Scatterers by Suitable Inverse Processing of GPR Data

G. Valerio[1], F. Soldovieri[2], P. M. Barone[3], S. E. Lauro[3], E. Mattei[3], E. Pettinelli[3], D. Comite[4], and A. Galli[4]

[1] I.E.T.R., Institut d'Electronique et de Télécommunications de Rennes – University of Rennes 1, Rennes, France
[2] IREA, Istituto per il Rilevamento Elettromagnetico dell'Ambiente – C.N.R., Naples, Italy
[3] Department of Physics "E. Amaldi" – Roma Tre University, Rome, Italy
[4] Department of Information Engineering, Electronics and Telecommunications – 'Sapienza' University of Rome, Rome, Italy

***Abstract*—The ability to reconstruct the correct shapes of buried scatterers in geophysical and planetary applications is addressed here, based on the use of Ground-Penetrating-Radar (GPR) investigations. Objects of different shapes and materials have been considered and an extensive analysis has been carried out both from a campaign of measurements, performed with a commercial GPR system, and from accurate numerical simulations, obtained with ad-hoc implementation of a CAD tool. Thanks to the use of a frequency-domain tomographic inversion algorithm, useful information about the shape characteristics of the detected objects could be recovered, even in critical cases of scatterers and measurement extents comparable to the wavelengths of the probing signal.**

Keywords - GPR instrument; radargrams; CAD simulations; scattering from objects; inverse scattering techniques.

I. Introduction

Recovering information on position and shape of buried objects is of paramount importance in fields such as geophysics, planetary exploration, environmental protection, archaeological investigations, mine clearance, etc. This kind of studies is usually performed through electromagnetic techniques, in particular using different kinds of ground-penetrating-radar (GPR) instruments [1]. In this connection, it is desirable to have methods that allow one to recognize different kinds of canonical shapes, even having a reduced cross section (e.g., wedges, corners, curved surfaces). This issue is addressed here and it is shown how the use of a microwave tomographic approach [2],[3] is suitable to achieve a shape estimation of the scatterers.

The analysis is developed by considering both experimental and numerical data in a scenario challenging to tackle, since both the targets and the scene extent are comparable to the probing wavelengths. Choices of the relevant electromagnetic parameters, operational frequencies, and shapes of objects here are related in particular to the investigations performed in the framework of the "WISDOM" project [4]. This includes the design and the characterization of a GPR system, to be mounted on the bottom of a rover exploring the Martian equatorial shallow surface. The rover will be equipped with a drilling system; in order to collect samples of soils to be analyzed on site, the GPR should recognize the safest places (i.e., with no rocks in the first meter of the subsurface) to be drilled.

II. Experimental and Numerical GPR Analyses

A. Laboratory experimental setup

The experimental setup consists of a 150×100×30 cm dielectric box ('basin') made of fiberglass, that can be filled with liquid and/or granular materials [5]. GPR measurements were performed using a mixture of glass beads (400-800 μm) as a background material in which targets having different geometries can be buried. The *laboratory setup* including the GPR instrument is illustrated in Fig. 1(a).

In the measurements considered here, the targets are made of hard wood and wrapped with aluminium foils, in order to simulate metallic objects. The objects were buried in pairs (always at about 9 cm depth from the surface), along the major (x) axis of the basin (central line). We started acquiring scattering data for a cube (9×9×9 cm) and a square-base pyramid (9×9×10 cm height); then for a sphere (Ø 8 cm) and a cone (base Ø 9×10 cm height); and, finally, for a cylinder (base Ø 5×10 cm height) and a parallelepiped (5×5×10 cm), positioned first parallel and then perpendicular to the GPR profile. A number of radar profiles were collected using a bistatic GPR system (*PulseEkko Pro*, Sensors and Software, Inc.) equipped with 1 GHz bandwidth antennas working at the central frequency of 1 GHz. For each couple of rocks, the GPR data were acquired performing scanning with different configurations: one with the *Tx/Rx* antenna pair placed parallel to the scanning direction along the basin, and the other with the antenna pair placed perpendicularly to the scanning direction. Each antenna can also be rotated by 90° with respect to the other. The best detection is in general observed with the antennas parallel to the scan line. A relevant example of a measured radargram is shown in Fig. 1(b), in the presence of two scatterers, with cubic and pyramidal shapes. In the following, all the shape reconstructions will be referred to this type of configuration.

B. Numerical Simulations

The experimental setup described above has also been simulated by means of a suitable implementation of a CAD tool for high-frequency electromagnetic analyses, *CST Microwave Studio*. In order to obtain results consistent with the measured data, a pair of UWB printed antennas have expressly been designed and simulated, having the same bandwidth of the commercial GPR system (0.5-1.5 GHz) [5].

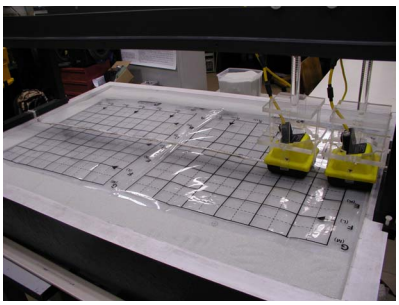

(a)

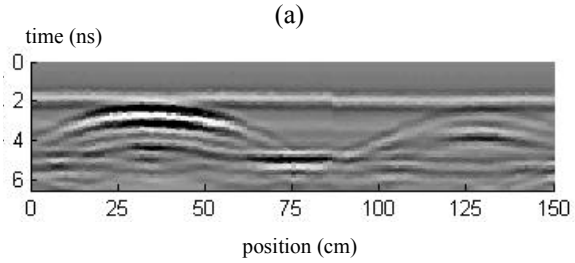

(b)

Figure 1: Our laboratory setup: (a) a commercial GPR instrument placed on a basin filled with a glass-bead mixture; (b) a measured radargram (scanning along the basin length) in the presence of two buried scatterers: a 9×9×9 cm cube and a pyramid (with the square base as for the cube and height h = 10 cm), buried at the left and at the right of the box, respectively.

A specific host medium has been simulated, analogue to the mixture for the experiments. The equivalent relative dielectric constant of the medium is evaluated on the basis of the radargrams in Fig. 1, and, independently, with time-domain reflectometry measurements (TDR) [6],[7]. A resulting real part of the relative permittivity ε_r = 3.2 is obtained, consistently with preliminary investigations in [7],[8], where several synthetic Martian soils simulants were analyzed. From those data the attenuation of the present sand is also extrapolated, being less than 0.1 dB/m. Such a low attenuation is due to the absence of magnetic minerals in the sample soil, which would lead to a relative magnetic permeability different from unity and to considerably higher losses. The scenario of a magnetic soil is examined with more details in [5],[8], where the detectability of buried basaltic rocks and the spatial resolution of the radar system is assessed.

In order to compare numerical results of the simulated setup with the measurements performed in the experiments discussed in the previous subsection, objects with the same shape as those used in the measurement campaign have been examined at the proper locations in the hosting medium. The antennas are swept along a line on the surface of the soil, in a bistatic configuration with a fixed offset (19 cm). For each position, a Gaussian pulse is radiated by the transmitting antenna and the signal at the output of the receiving antenna is collected. Each received trace consists of a first 'direct' signal, guided by the soil interface, due to the direct path between the transmitting and the receiving antenna. This signal is followed at a later time by the signal scattered by the buried object. If superficial roughness is neglected, as reasonable if antennas are moved in contact with a smooth sandy soil, the 'direct' signal is the same for any position along the observation domain, and can be evaluated numerically with an additional simulation of the pair of antennas in the absence of any buried rock. In the results shown here, the 'direct' signal is subtracted from each trace (such regularization is named 'background removal'), in order to highlight the scattering contributions of the rocks rather than the noise of the surrounding environment [5].

After this background removal, the set of all the received traces leads to a *simulated radargram*, also depictable in gray scale, which can be compared to the results of the measurements. Such simulated environment thus allows for inexpensive tests with flexible choices of the physical and geometric parameters. In Fig. 2, two examples of the results achieved with our numerical implementation are shown through this scattered-field radargram form, considering the canonical shapes of scattering metallic objects in Fig. 1: cube in Fig. 2(a) and pyramid in Fig. 2(b).

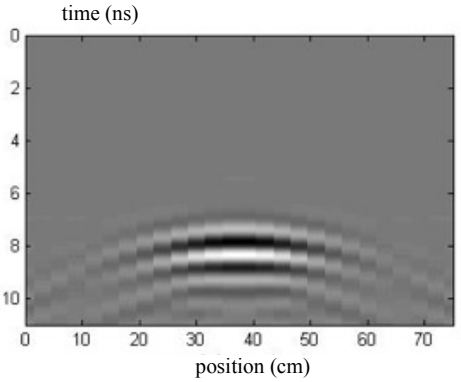

(a)

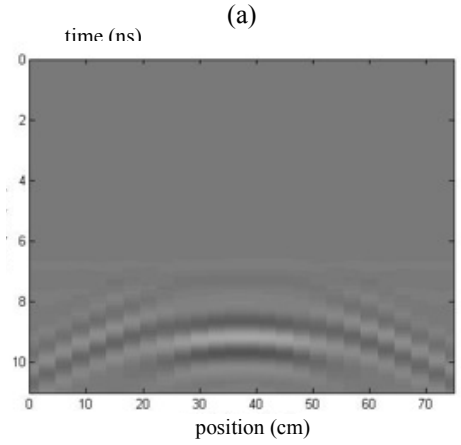

(b)

Figure 2: Examples of simulated GPR radargrams derived through our CAD implementation, due to buried scatterers with the same geometries of Fig. 1: (a) a metallic 9×9×9 cm cube; (b) a metallic pyramid (with the square base as for the cube and height h = 10 cm).

III. Inverse Problem and Results

The GPR experimental and numerical data have been processed by means of a *microwave tomographic approach* based on the Born Approximation (BA), which allows us to linearize the relevant inverse problem [2]. This type of approximation is particularly suitable here, as we consider single objects (numerical simulations) or well spaced objects (experiments) with negligible mutual interactions.

As is known, BA performs the quantitative reconstruction of the target only when associated to a full view configuration and for weak scatterers. In our cases, we deal with strong scattering targets, and the exploitation of BA is considered suitable once one renounces to accurate electromagnetic characterizations and aims only to detect and estimate the geometry of the target [3]. The inverse problem amounts to the inversion of a linear integral equation relating the "contrast function" (representing the target) to the scattered-field data. Inversion is carried out by means of the Truncated Singular Values Decomposition that permits us to achieve a stable solution [2],[3].

As a test of the effectiveness of the approach, we present some tomographic reconstructions given in terms of the normalized amplitude of the contrast function (the relevant 2D spatial distribution is plotted with a colour scale). The first results shown here in Fig. 3 are derived by processing the regularized data from the simulated setup as in Fig. 2: Fig. 3(a) refers to the cube and Fig. 3(b) to the pyramid. It can be seen how these two geometries have their counterpart in the rather different shapes of the relevant contrast function. In particular, the position of the cube is properly located, with a well visible upper interface. The tip of the pyramid can also be reconstructed, the difference between a flat interface and a wedge being fully recognized.

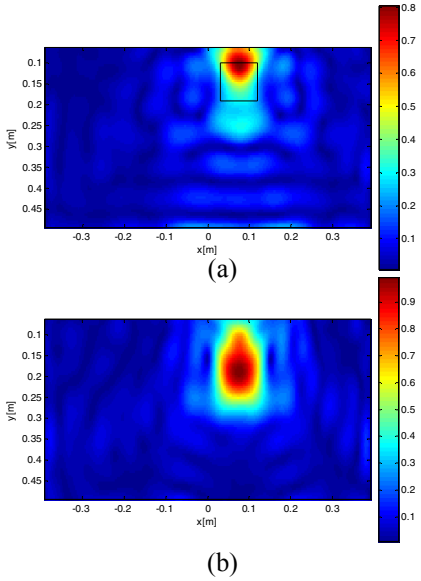

(a)

(b)

Figure 3: Microwave tomographic reconstruction of scatterers from simulated radargrams as in Fig. 2: (a) cube; (b) pyramid.

We have also considered the tomographic reconstruction by starting from the raw data of the measured radargrams, as in Fig. 1(b) for the cube and pyramid. The relevant result shown in Fig. 4 enables us to detect and well localize the two targets and the bottom of the dielectric box. Moreover, a different reconstruction is given for the two targets. The cube is retrieved at about $x = -30$ cm and the spot's extent has a dimension almost equal to the cube's side. The bottom of the box is retrieved at the middle of the scene. The pyramid is retrieved at about $x = +45$ cm as two spots; the first one representing the wedge of the pyramid since the deeper spot accounts for the bottom of the structure.

It is worth noting that the considered test cases are challenging. In fact, a multi-bistatic configuration is adopted with an offset between *Tx* and *Rx* antennas (about 20 cm) larger than the depth of the target (about 10 cm). Also, the signal bandwidth is 1 GHz and the probing wavelength in the filling medium at middle frequency is around 15 cm, so that the target extents are comparable with the resolution limits imposed by the measurement configuration.

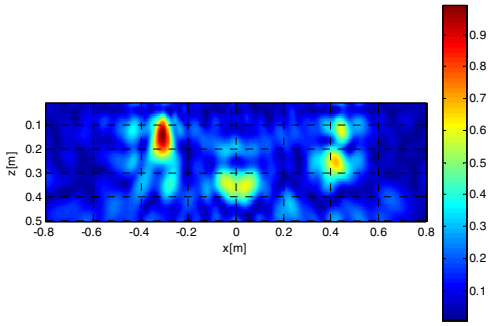

Figure 4: Tomographic reconstruction of scatterers from measured radargrams as in Fig. 1: the cube-pyramid experiment.

IV. Conclusion

The achievement of information on scatterers' shape in particular challenging GPR practical conditions has been analyzed, based on data from experimental and simulated radargrams, inverted with a suitable tomographic approach.

Acknowledgment

This work has been financially supported by the Italian Space Agency through contract ASI-INAF n. I/029/08/0.

References

[1] D. J. Daniels (Ed.), *Ground penetrating radar*. IEE Press, 2004.

[2] G. Leone and F. Soldovieri, "Analysis of the distorted Born approximation for subsurface reconstruction: truncation and uncertainties effects," *IEEE Trans. Geosci. Remote Sensing*, vol 41, pp. 66-74, Jan. 2003.

[3] E. Pettinelli, A. Di Matteo, E. Mattei, L. Crocco, F. Soldovieri, J. D. Redman, and A. P. Annan, "GPR response from buried pipes: measurement on field site and tomographic reconstructions," *IEEE Trans. Geosci. Remote Sensing*, vol. 47, pp. 2639-2645, Aug. 2009.

[4] V. Ciarletti, C. Corbel, D. Plettemeier, P. Caïs, S. M. Clifford, and S. E. Hamran, "WISDOM GPR designed for shallow and high-resolution sounding of the Martian subsurface," *Proc. IEEE*, vol. 99, pp. 824-836, May 2010.

[5] G. Valerio, A. Galli, P. M. Barone, S. E. Lauro, E. Mattei, and E. Pettinelli, "GPR detectability of rocks in a Martian-like shallow subsoil: a numerical approach," *Planet. Space Sci.*, 10 pp., doi: 10.1016/j.pss.2011.12.003, 2011.

[6] E. Pettinelli, A. Cereti, A. Galli, and F. Bella, "Time domain reflectometry: calibration techniques for accurate measurement of dielectric properties of various materials," *Rev. Sci. Instrum.*, vol. 73, pp. 3553-3562, 2002.

[7] E. Pettinelli, G. Vannaroni, A. Cereti, F. Paolucci, G. Della Monica, M. Storini, and F. Bella, "Frequency and time domain permittivity measurements on solid CO2 and solid CO2–soil mixtures as Martian soil simulants," *J. Geophys. Res.*, vol. 108, 11 pp., Feb. 2003.

[8] E. Pettinelli, P. Burghignoli, A. R. Pisani, F. Ticconi, A. Galli, G. Vannaroni, and F. Bella, "Electromagnetic propagation of GPR signals in Martian subsurface scenarios including material losses and scattering," *IEEE Trans. Geosci. Remote Sensing*, vol. 45, pp. 1271-1281, May 2007.